Renewable Energy 93 (2016) 101–114

Contents lists available at ScienceDirect

Renewable Energy

journal homepage: www.elsevier.com/locate/renene

Design and experimental performance of brackish water reverse osmosis desalination unit powered by 2 kW photovoltaic system

M.A. Alghoul [a, b, c, *], P. Poovanaesvaran [c], M.H. Mohammed [c], A.M. Fadhil [c], A.F. Muftah [c], M.M. Alkilani [d], K. Sopian [c]

[a] Energy and Building Research Center, Kuwait Institute for Scientific Research, P.O. Box 24885, Safat 13109, Kuwait
[b] Center of Research Excellence in Renewable Energy (CoRe-RE), Research Institute, King Fahd University of Petroleum and Minerals (KFUPM), Dhahran 31261, Saudi Arabia
[c] Solar Energy Research Institute, Universiti Kebangsaan Malaysia, 43600 Bangi, Selangor, Malaysia
[d] Mechanical Engineering Department, Al Jabal Al Gharbi University, Libya

ARTICLE INFO

Article history:
Received 26 September 2015
Received in revised form
2 January 2016
Accepted 5 February 2016
Available online xxx

Keywords:
Desalination
Brackish water reverse osmosis ((BWRO) unit
PV power system
Design and sizing
Experimental validation and performance

ABSTRACT

Small-scale brackish water reverse osmosis (BWRO) desalination units are not a major commercial success compared to its large-scale counterpart. Integrating renewable power systems with small-scale units would theoretically aid in their deployment and subsequent commercial success. In fact, RO units are constructed using a modular approach; this would allow them to adapt to a renewable power supply. Small-scale PV-RO would be a promising form of desalination system in remote areas, where BW is more common. The aim of this study is to quantify the effect of climatic-design-operation conditions on the performance and durability of a PV-BWRO desalination system. A small-scale unit is designed, constructed, and tested for 6 months. The design was limited to a 2 kWp PV power system, five different membranes, a feed TDS of 2000 mg/l, and a permeate TDS of less than 50 mg/l. Data pertaining to solar radiation and temperature were subsequently analyzed to determine their respective influences on current and future operations of the unit. The results showed that the optimum RO load, membrane type, and design configuration were 600 W, (4″x40″ TW30-4040), and a two-stage configuration, respectively. The PV system was able to supply the load without any significant disturbances; while the RO unit showed stable levels of permeate flow and salinity. Operating the PV-BWRO system for 10 h during the day would produce 5.1 m3 of fresh water at a specific energy of 1.1 kWh/m3. It was confirmed that there are many hours of high temperatures during the operation of the PV module (exceeding 45 °C) and battery room conditions (exceeding 35 °C), both of which could negatively affect the power output and battery autonomy. This negative effect is compounded annually; therefore, optimizing thermal regulation of PV modules and battery bank room conditions is essential in maintaining excellent operating temperatures.

1. Introduction

Despite the biannual monsoon torrent, fresh water is a scarcity in the rural areas of Malaysia. The people living there are five times more likely to lack access to potable water compared to their urban counterparts UNICEF & WHO [1]. The lack of potable water results in illnesses and the loss of productivity. Children are especially vulnerable, as they are not strong enough to fight diarrhea, dysentery, and other illnesses. A study was carried out involving school children living in rural communities in Lipis and Raub districts of Pahang, and the results indicated that Blastocystis (intestinal protozoan) is prevalent amongst rural children; the source of this illness is traced back to their drinking water Abdulsalam et al. [2]. Therefore, desalination is required to allow residents to enjoy better living standards.

The most widely used methods for desalination include thermal and membrane processes. Reverse osmosis (RO) is a membrane process technique, which is more popular compared to the conventional thermal process technology, such as Multi Stage Flashing (MSF) and Multi Effect Distillation (MED). One of the biggest

* Corresponding author. Energy and Building Research Center, Kuwait Institute for Scientific Research, P.O. Box 24885, Safat 13109, Kuwait.
E-mail address: dr.alghoul@gmail.com (M.A. Alghoul).

http://dx.doi.org/10.1016/j.renene.2016.02.015
0960-1481/

advantages of the RO system is its low energy consumption compared to all other desalination systems [3–5]. Energy consumption contributes up to 45% of the total cost of an RO system Zhu etal [6]. The investment costs for energy supply of the RO systems in rural areas makes up almost 60% of the total budget Espino et al. [7].

A significant amount of energy in the RO unit is used for the initial pressurization of the feed water Alghoul et al. [8]. The initial pressurization for brackish water occurs at ~27 bars, whereas seawater desalination requires a high-pressure of ~70 bar Abdallah et al. [9]. RO systems are flexible in the context of feed water quantity and quality, site location, and system start-up and shut-down [10,11]. The critical factors for sizing of the RO unit are the daily per capita consumption, total population, as well as hours of operation of the unit per day Tzen et al. [12]. The optimum RO system would have high recovery ratio (maximum permeate flow and minimum permeate salinity) at minimum feed pressure, and a reasonable number of membrane modules. With a low feed pressure, the life span of the membrane could be increased; however, this could in theory compromise the recovery ratio Sarkar et al. [13].

Despite the fact that small-scale brackish water reverse osmosis (BWRO) desalination units are simple desalination systems with minimum maintenance requirement, they have not seen major commercial success compared to large-scale desalination systems Ayoub and Alward [14]. Therefore, increasing the deployment of small-scale BWRO desalination systems is still a priority. The fact that the RO systems are constructed using a modular approach allows them to adapt to a renewable energy supply Lindemann [10]. Therefore, integrating renewable power system with a small-scale RO system would improve their commercial penetration [15–17]. PV-BWRO systems can be regarded as a promising desalination option in remote areas. In literature, there are many case studies of small-scale PV-BWRO desalination units at different locations around the world, such as in Egypt, powered by 19.84 kWp PV system Maurel [18], Spain (23.5 kWp) Peral et al. [19], Algeria (2.7 kWp) Kehal [20], Brazil (1.1 kWp) de Carvalho [21], Portugal (0.5 kWp) Joyce et al. [15], Oman (3.25 kWp) Loureiro D et al. [22], and Iraq (5 kWp) Al Suleimani and Nair [23]. According to Garcia-Rodriguez [24], photovoltaic energy is used to power small-scale BWRO desalination systems, resulting in a water production of up to 60 m3/day. Herold et al. [25] demonstrated a small PVRO system, which produces 1 m3/d of water at remote areas that lack grid electricity, have higher specific energy consumptions compared to its medium and large counterparts, but its initial cost is still lower compared to other desalination systems. Gocht et al. [26] investigated the technical feasibility and cost benefits of a PV-powered brackish water small-scale desalination plant in a rural area. They confirmed the socio-economic feasibility of desalination that is provided by a transient and discontinuously operated PV-coupled RO system. Generally, continuous operation is defined as a daily operation, whereas discontinuous operation is limited to 5–10 h a day, depending on the location and need for optimum operating hours. Continuous operating systems require large battery banks to provide power at night or during cloudy times; this requirement, however, increases the total costs. Another option is to store water in a storage tank to reduce the cost and the number of batteries needed [27].

The combination of renewable energy sources and water desalination systems require addressing challenges in the operation of an integrated system, specifically, the problem of unexpected fluctuations in energy production of a solar energy generation system requiring quick start units to cover shortfalls or absorb unscheduled energy generation [29]. One way to deal with these issues is through the use of integrated energy generation systems using solar energy with other renewable energy options. In recent years, there have been many researchers working on “smart” electrical grids, which is an extension of our traditional electrical grid, with distributed, medium-scale renewables-based energy generation systems and digital technologies, to meet the increasing energy demand and environmental regulations [28]. A supervisory model predictive control (MPC) was designed by Wei Qi et al. [29] to optimally operate an integrated solar/RO system, and the “smart” electrical grid able to coordinate the solar subsystems and the battery to provide enough energy to the RO subsystem to fulfill water production demands.

The main aim of this study is to learn and gain insights into the effect of climatic, design, and operation conditions on the BWRO and PV systems' performance and durability. Therefore, a small-scale BWRO unit powered by a 2 kWp PV system was designed, constructed, and tested. The RO unit was designed to treat a feed salinity of up to 5000 mg/l at permeate salinity values of less than 50 mg/l. Experimental work pertaining to this project will be conducted at the solar field of the National University of Malaysia (UKM), Bangi, Malaysia, which is located at 2° 56′ N, 105° 47′ E, corresponding to a GMT +08:00. Outdoor experimental performance of PV-BWRO system will be determined for multiple operating modes. The cost of a PV-BWRO desalination system, in the context of research purposes, will be detailed as well. Images pertaining to the PV and RO test units are shown in Fig. 1.

2. Materials and methods

2.1. Water salinity

The characteristics of the feed water vary from location-to-location, and to document these differences, samples were collected and tested from multiple sites at different distance from the sea at Mersing, Johor. The values were subsequently averaged and summarized, and the results are tabulated in Table 1. These data allowed us to conclude that the tested water was brackish.

2.2. Solar resources

Solar radiation is a geographically dependent feature. It is essential that we are aware of the amount of solar radiation received at a particular location at any given time [30]. Solar radiation in Malaysia is highest in the north of the Peninsular and the state of Sabah, with recorded values of 5.2 kW/m2, while the minimum solar irradiation is 4.2 kW/m2, recorded in the south of the Peninsular and the state of Sarawak [31]. The annual average solar radiation at this area is 4.794 kW/m2/day.

Fig. 1. Photo of PV and RO test units located in the solar field @UKM, Malaysia.

Table 1
Water salinity at different distance from sea at Mersing, Johor, Malaysia.

Distance from sea	TDS (mg/l)
1.5 km	14,600
4 km	13,400
11 km	1000

2.3. Components of PV-BWRO desalination system

The test unit consists of a PV power system, BWRO desalination unit, and two measurement systems. The PV components that are used in the design and building of the test unit are multi-crystalline PV modules (125 W), batteries (12 V, 200 Ah, 2.4 kWh), charge controller, converter, and communication modules. The RO unit consists of pressure vessels, stainless steel high-pressure pump, multi-media filter, sediment filter, and anti-scalant dosing systems. The measurement systems consist of 2 data acquisition for PV and RO systems, including sensors for (temperature, irradiance, TDS, pH, pressure and flow meters), PV data logger, and an RO data logger. Table 2 summarizes the components, brands, models, and specifications.

The PV modules were purchased from Solar-TIF, which is a partner company of the National University of Malaysia. The capital and replacement cost of the adopted PV modules is assumed to be USD 1.02/W [18], encompassing shipping, tariffs, installation, and dealer mark-ups.

Batteries are included in the system's analysis; they provide a stable current supply and store energy for use during cloudy weathers. Power produced by the PV modules is in DC form, and it must be converted to AC in order to power the pumps. This can be done using a power converter. The capital and replacement cost of one battery is assumed to be 438$ [18], the installation and replacement cost of a power converter is 714$/kW [18], and the efficiency of the converter is assumed to be 85%. Fig. 2 describes the main components of PV & RO systems.

2.4. Methods

The following tools were used to realize the objectives of this study:

- HOMER simulation tool [32], which is an energy optimization model for hybrids and stand-alone power systems. It was used to determine the maximum load that could be powered by a 2 kWp PV system.
- Reverse Osmosis System Analysis (ROSA) [33], which is a sophisticated reverse osmosis (RO) design program that predict performances based on types of membranes. It was used to determine the type of membrane that will result in the optimal design configuration for a BWRO unit, based on the load that can be powered by a 2 kW_p PV system.
- Statistical test tools

Experimental validation is a necessary step for the acceptance of the simulation results. Two statistical test tools are used to confirm the agreement between the simulated and experimental results, namely coefficients of determination (R^2) [34] and the efficiency (EFF) statistical test [35].

i. Coefficient of determination (R^2).

$$R^2 = 1 - \frac{\sum_{i=1}^{N}(obs_i - sim_i)1^2}{\sum_{i=1}^{N}(obs_i)r^2}$$

R^2 is always positive between 0 and 1.

ii. EFF, which was proposed as the best overall measure of agreement between the measured and simulated values.

$$EFF = 1 - \frac{(Mean\ Square\ Error\ (MSE))}{(Variance\ of\ experimental\ data)}$$

Successful EFF values are between 0 and 1; a test result with negative EFF values cannot be recommended. In other words, the MSE must be less than or equal to the variance of the measured values for the model to be accepted. Preferable values for both statistical tools are those that are close to unity, because these values are indicative of a near perfect model.

3. Design and sizing of PV-BWRO desalination system

Table 3 lists the main design assumptions adopted in designing and sizing a PV-BWRO desalination system.

3.1. Determining the optimum load of the BWRO unit powered by 2 kWp PV system

2 kWp PV modules were purchased based on the allocated fund. The performance of a solar panel depends on the orientation and the optimal tilt angle. An improper orientation or tilt angle of the solar panel would eventually lead to losses in power, and subsequently poor return of investment [23]. The tilt angle was simulated using the HOMER simulation tool, as per Yadav and Chandel [36]. The results showed that the optimum tilt angle is 14° [21]. reported that placing the panels at an angle between 5 and 15° allowed rain water to remove dust and dirt from the surface of the PV panel.

The HOMER simulation tool is used to evaluate the techno-economic choices, comprising of the optimum load, number of batteries, and inverter size under different operating hours during the day. Simulation results showed that a 2 kWp PV system can produce 7.67 kWh/day, totaling to 2800 kWh/yr at (2° 56′ N, 105° 47′ E).

A PV system does not need to serve occasional large loads. Extreme cases, such as several cloudy days, rarely occur, and if it does, the RO desalination unit can be built with a storage tank that stores water for use in emergencies. Therefore, allowing a portion of the annual load to go unserved will reduce the number of

Table 2
Specifications of PV-BWRO desalination components.

Component	Brand	Model	Specification
PV modules	SolarTIF	STF-130P6	130W
Charge controller	TriStar	MPPT-45	45A
Inverter	Studer	XTM 2600-48	48VDC
Battery	GP	GPP 122000	12V, 200Ah
Membrane types	Filmtec from Dow	(SW30HRLE-4040, BW30-4040, TW30-4040, SW30HRLE-440i and SW30XLE-400i)	41 bar (maximum)
Feed pump	Procon	111A125F11AA	8.3 bar

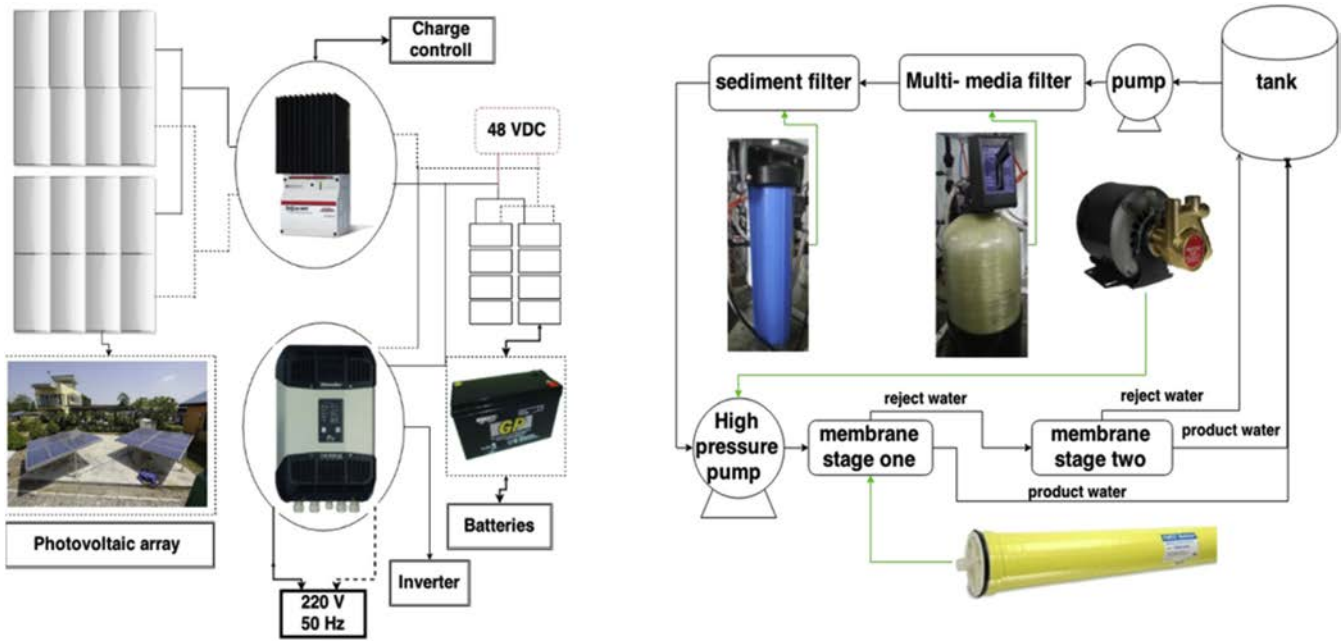

Fig. 2. Main components of PV & RO systems.

batteries needed, and accordingly, the capital and operational costs. Typically, the annual unserved load falls between 0.5%–4% [32].

The feasible techno-economic results showed that the range of RO load that can be powered by a 2 kWp PV module is between 400 W and 800 W with unmet electrical load of 0.5% and 4% respectively. The feasible number of batteries is between 4 and 16 units. To determine the optimum number of batteries and load, further analysis need to be done under different operating hours of daytime. Fig. 3 shows the number of batteries vs. loads' power at multiple operating hours (5–7 h). As shown in the figure, the reasonable number of batteries for load operations is 4 and 8. However, (8) batteries seem prudent. After this step, the optimum load needs to be determined. The optimum load is the maximum load that can operate 7 h by a 2 kWp PV system using 8 batteries during daytime. It can be seen that the optimum load is 600 W. The batteries' autonomy was found to be 46.5 h.

Based on the aforementioned results, the feasible converter is found to be (2 kW), and can operate for 3650 h/yr, and convert 2343 kWh/yr, thereby producing 2109 kWh/yr at an electrical loss of 234 kWh/yr. Table 4 shows power transformation and losses via the converter.

3.2. Optimum membrane type, number of elements and design configuration of BWRO unit

The optimum load (600 W) that can be powered by a 2 kWp PV system during daytime is determined. The ROSA simulation tool is used to determine the optimal membrane type, design configuration, and the number of membrane elements to produce fresh water under 600 W load and a permeate TDS of less than 50 mg/l.

In this round of analyses, different membranes (SW30HRLE-4040, BW30-4040, TW30-4040, SW30HRLE-440i and SW30XLE-400i) were implemented to determine which of them require the lowest power to produce similar amounts of permeate flow. This procedure is evaluated under single-stage design, with one pressure vessel containing one element. Under this design configuration, it is easy to predict the membrane type/types that results in lowest and highest powers at similar permeate flow. It is also easy to predict the range of permeate flow that can be powered by the designed load (600 W).

The choice between single-stage configuration and two-pass configuration for the same level of total water recovery and salt rejection depends on the lowest energy consumption, which can be compared when the applied pressure is equal to or more than thermodynamic cross flow limit without energy recovery devices Zhu et al. [6]. Generally, most authors agree that a two-stage system is more energy efficient compared to a single-stage system, however, Zhu et al. [6] pointed out that for brackish water, a single-stage

Table 3
The design scope/limitation/assumptions adopted in this study.

Parameters	Value
Annual solar radiation	4.794 kW/m^2
PV array power capacity	2kW$_p$ (max)
Capacity shortage	Max. 5%
Unmet electrical load	0.5–4%
Implemented membranes	5 types
Feed TDS	2000 mg/l

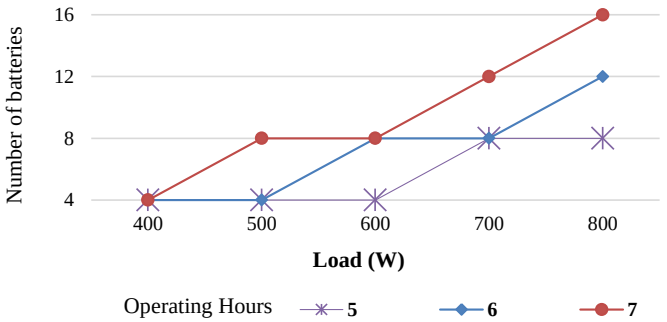

Fig. 3. Number of batteries versus load at different operating hours during daytime.

Table 4
Power transformation and losses by converter.

Quantity	Inverter	Units
Hours of operation	3650	hrs/yr
Energy in	2343	kWh/yr
Energy out	2109	kWh/yr
Losses	234	kWh/yr

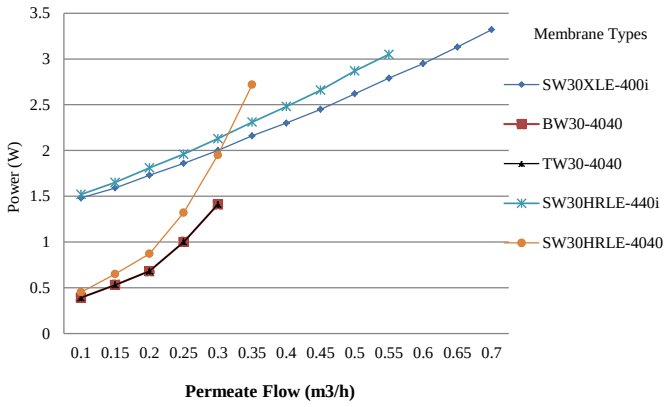

Fig. 4. Power versus permeate flow at different membrane types.

system is more cost effective system than a two-pass system. A two-pass system would be energy efficient than a single-stage system if water recovery of single stage were below 50%.

Fig. 4 shows the required load power of different membrane types versus the permeate flow under a feed TDS of 2000 mg/l. It can be seen that TW30-4040 and BW30-4040 show the lowest power requirement, and they overlap each other, followed by SW30HRLE-4040. Under 600 W, they can produce permeate flow of less than 0.15 m3/h. SW30XLE-400i and SW30HRLE-440i show the highest power (far from 600 W).

In this study, TW30-4040 was chosen because it can function under the designed load (600 W). Also, it is able to operate at very low pressure and can be cleaned over the widest pH range (1–13). It is made of the thickest feed spacer (34 million), and is less affected by fouling.

Besides the load power limitation of the RO unit (600 W), the product's water salinity should also be under 50 mg/l Fig. 5 shows the permeate salinity versus load power at different design configurations. Symbols {(1), (2), (3) and (4)} represent one stage design of one pressure vessel, with 1, 2, 3, and 4 membrane elements, respectively. Symbol (1–1) represents two-stage (at each stage one pressure vessel with one membrane element). Symbol (2–2) represents two-stage (at each stage one pressure vessel with two elements), and symbol (2–1) represents two-stage (at 1st stage one pressure vessel of two elements and at the 2nd stage one pressure vessel of one element). As shown in Fig. 5, all design configurations were able to produce water with permeate salinities below 50 mg/l under a load of 600 W.

Fig. 6 shows the amount of permeate flow and the cost of membrane and pressure vessels versus different design configurations under a feed TDS of 2000 mg/l. It is seen that the product flow is directly proportional to the number of membranes. Also, it can be seen that product flow is similar if the total number of membrane elements used is still the same under single or two-stage modes, while the cost increases as additional numbers of membrane elements and pressure vessels were added. As shown in Fig. 6, design configuration (1) showed the lowest cost (500$) but at the lowest permeate flow (0.28 m3/h), so this choice will be abandoned in this study. The maximum permeate flow is 0.79 m3/h and 0.8 m3/h, and it is possible only under design configurations (4) and (2–2), respectively. Design configuration (2–2) was the most expensive (2400$), which is why it will be abandoned in this study as well.

Comparing design configuration (1–1) with (2), (3), and (4); (1–1) is a two-stage design, the cost is the least and with reasonable permeate flow (0.52) m3/h concurrently. Besides that, recycling it at the 2nd stage can minimize the amount of rejected water. Based on that, design configuration (1–1) seems to be more attractive, and will be adopted in this study as the optimum design configuration in terms of cost, reasonable permeate flows and minimum amount of rejected water. The product salinity for (1–1) is 21.1 mg/l, as shown in Fig. 5.

4. Test unit and measurement systems

Based on the simulation results obtained from designing and sizing of the PV and RO units, the components were identified, sourced, and purchased to build the system. The PV-BWRO test unit was operated for six months. During this period, different modes of operations were tested. The feed water for the experimental work is prepared using NaCl mixed in a water tank. It was recycled back into the water tank to keep the salinity levels constant throughout the experiment.

The RO unit is a two-stage design, consisting of multi-media and sediment filters as pre-treatment, high-pressure pump (600 W), 2 "Dow Filmtec TW30-4040, 4″x40″ membranes", and five types of

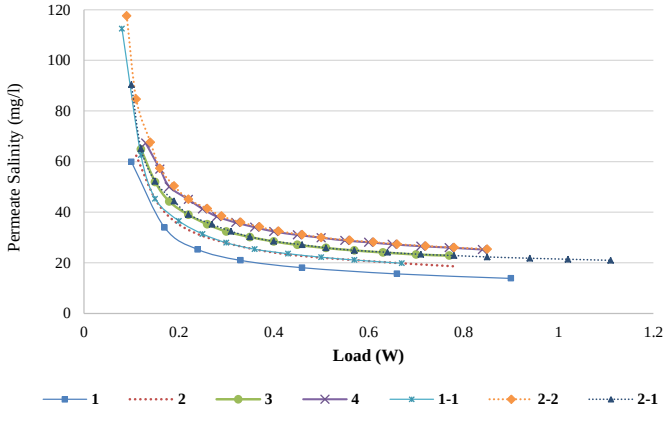

Fig. 5. Permeate salinity versus load power at different design configurations using TW30-4040 under feed salinity of 2000 mg/l.

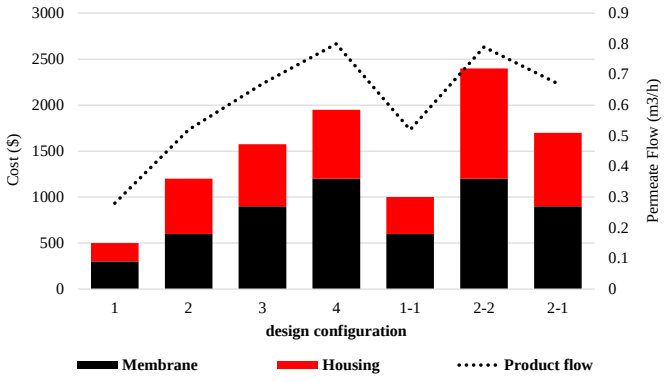

Fig. 6. Cost and permeate flow versus different design configurations of RO unit.

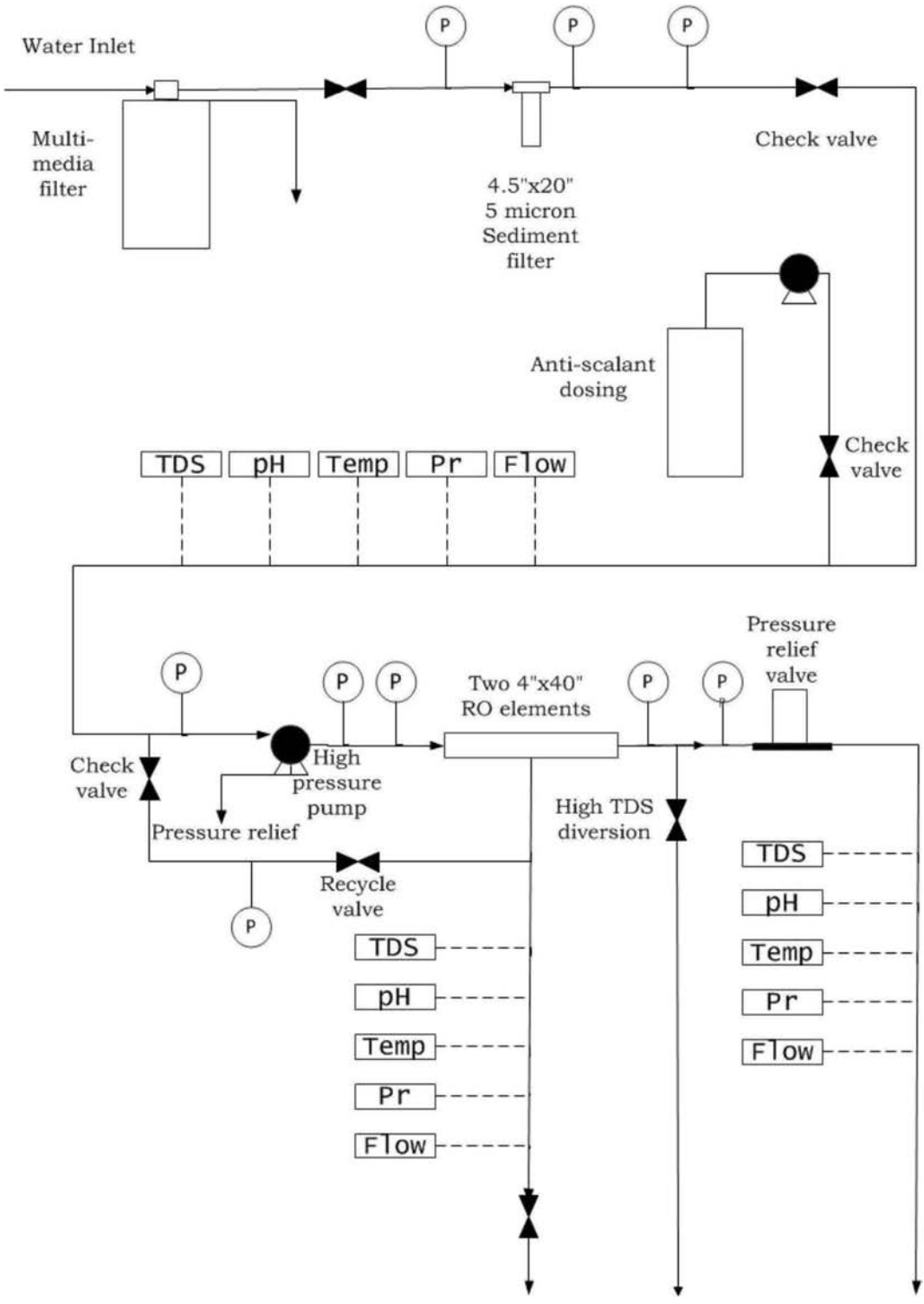

Fig. 7. Piping and instrumentation diagram of two-stage RO test unit using TW30-4040 membrane type.

sensors (TDS, pH, temperature, pressure, and flow meter at each channel). Fig. 7 shows the RO test unit's piping and instrumentation diagram (P&ID).

Fig. 8 shows the complete single-line diagram of the installed PV system. It shows how all the modules, batteries, inverter, charge controller, sensors, communication ports, and the load are connected to the data acquisition system.

5. Performance of BWRO desalination test unit

The PV power system was installed in March 2012, while the RO test unit was delivered after a one-year delay in April 2013. The installation of the PV-BWRO desalination system was completed in August 2013. After putting it together and conducting trial runs to determine its baseline, the experiment was started in November

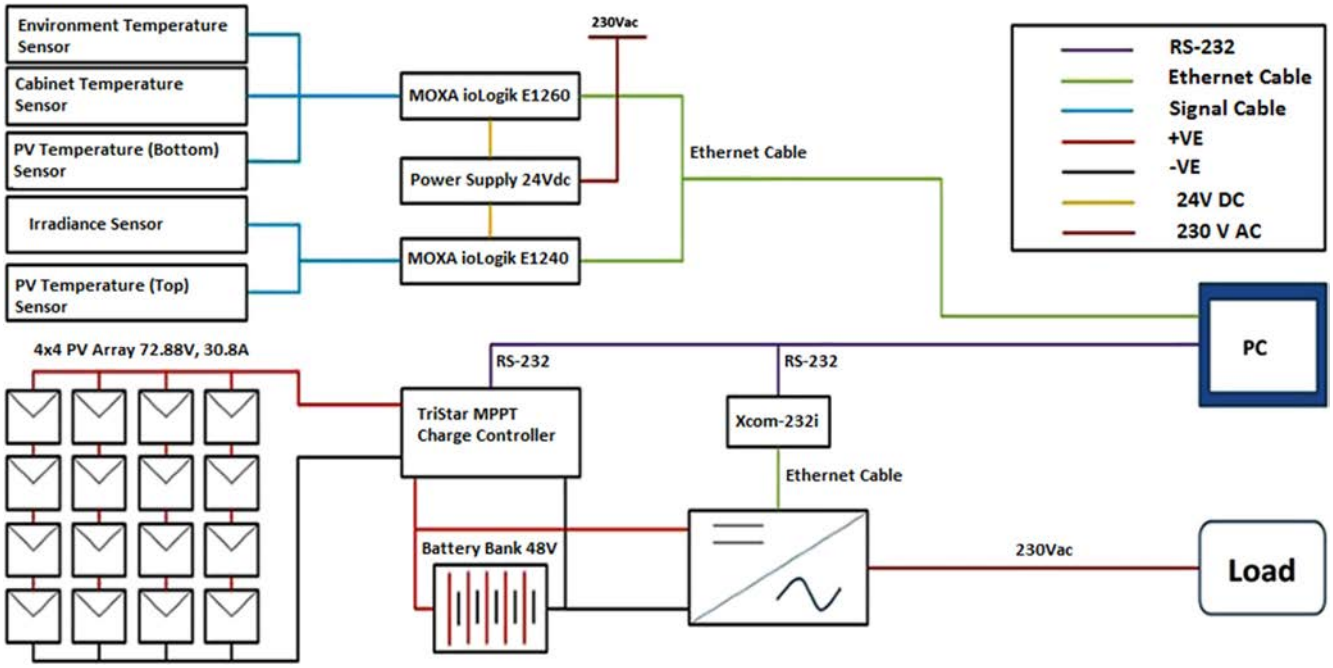

Fig. 8. Single-line diagram of the installed PV power system.

2013. Data collection continued for 6 months, up till April 2014.

5.1. Experimental validation

The aim of this sub-section is to confirm the agreement between the experimental results and the obtained results from the ROSA simulation tool. The following parameters are going to be selected for the experimental validation: permeate flow, permeate salinity and membrane pressure versus different feed salinities (500–5000 mg/l). In this round of analysis, the RO unit was operated continuously for 24 h; then, the measured values of each parameter were summed and averaged. Thereafter, the statistical tests were applied to determine the level of agreement between the average measured and simulated values.

In fact, the RO unit is designed to treat water with feed salinity of 2000 mg/l in mind, but for experimental validation purposes, the unit was pushed to operate under a feed salinity of up to 5000 mg/l

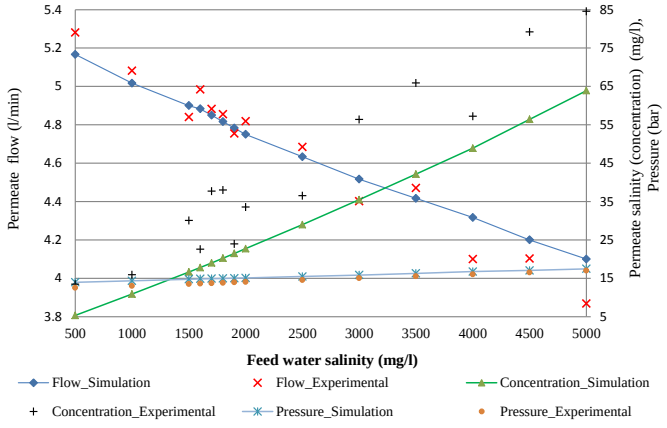

Fig. 9. Comparison between simulated and average measured permeate flow (left), permeate salinity and membrane pressure (right) versus feed salinity under single stage scenario of RO unit.

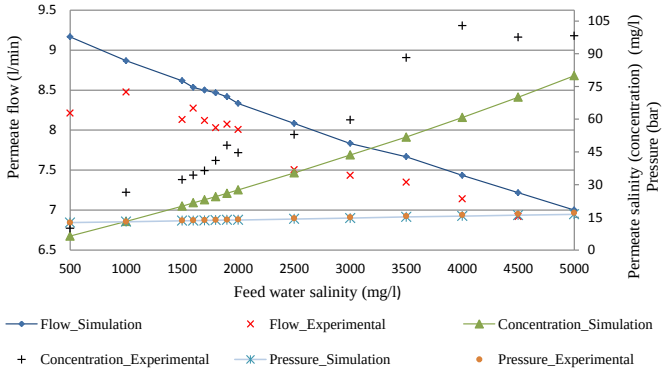

Fig. 10. Comparison between simulated and average measured permeate flow (left), permeate salinity and membrane pressure (right) versus feed salinity under two-stage scenario of RO unit.

with a TW30-4040 membrane. However, simulated permeate salinity values up till 80 mg/l is still a reasonable design assumption when using feed TDS′ exceeding 2000 mg/l Figs. 9 and 10 showed the simulated and average measured values under single and two-stage modes, respectively. Single-stage modes have one pressure vessel of one membrane element, while two-stage mode has one pressure vessel of one membrane element at each stage.

As shown in Fig. 9, the simulated and average measured permeate flow showed a linear reduction trend with the increase of feed salinity. On the whole, it was seen that the average measured permeate flow is higher than the simulated values vs. feed TDS of up to 3500 mg/l. After that, the average measured permeate flow was lower than the simulated value. The fluctuation of the measured permeate flow around the simulated permeate flow at different feed TDS′ could be attributed to the auto-adjustment by the RO system to keep the recovery constant. The recovery needs to be constant to keep the permeate salinity within the design's assumption. Also, part of the interpretation could be attributed to the membranes' limitation when it treats feed TDS′ higher than

2000 mg/l.

As shown in Fig. 9, the simulated and average measured permeate salinity exhibited linear incremental trend with increased feed salinity. On the whole, the average measured permeate salinity is relatively higher than the simulated values, with some fluctuation versus different feed salinities. The reason for that is that there are many parameters involved in the experimental measurements, and it is almost impossible for them to be similar to the assumed values for simulation purposes i.e. feed flow temperature and the difficulty of accurately measuring feed salinities as it fluctuates when mixed in a tank. Also, part of the interpretation could be attributed to the membranes' limitation when it treats feed water with higher TDS. It can also be seen from Fig. 9 that the membrane pressure showed slow linear increment trend, ranging from 14 to 17.5 bar, with the increase of feed TDS, while the average measured pressure is close to the simulated pressure.

Under a two-stage analysis, as shown in Fig. 10, the simulated and average measured permeate flow showed a linear reduction trend with increasing feed salinity. The average measured permeate flow is always relatively lower than the simulated values vs. the feed salinity, because it is not easy to measure permeate flow in a two-stage configuration, where the permeate flow from the first stage is combined with the permeate flow of the second stage. Feed flow, salinity, and pressure of second stage always fluctuate, and even a small fluctuation in one of these variables would affect permeate flows.

Average measured permeates salinity under two-stage scenario is similar to single-stage scenario, at both scenarios they exceed the simulated values. In a two-stage configuration, the permeate salinity of less than 50 mg/l can be achieved with feed TDS of less than 2500 mg/l. At higher feed salinities, permeate salinity increased even further. Beyond a feed TDS of 3500 mg/l, the fluctuation of permeate salinity is much higher, at ~100 mg/l. The observed fluctuation is due to similar factors, as discussed previously for a single-stage scenario. It can be seen also from Fig. 10 that the membrane pressure showed a linear increment trend, ranging from 12.5 to 17 bar with the increase of feed TDS; the average measured pressure overlaps the simulated pressure.

It is essential to statistically test the agreement between the measured and simulated results of the chosen parameters under single and two-stage scenarios. Table 5 summarizes the results of the statistical tests for the aforementioned scenarios. R2 and EFF statistical test tools showed satisfactory to excellent agreements between the measured and simulated values.

Based on Figs. 9–10 and Table 5, the statistical tests results confirmed the accuracy of the measured values with the simulated values, and consequently ensured the appropriateness of the design and sizing assumptions and procedures being adopted in this study.

5.2. Results of two weeks of continuous operation of the RO unit

In this round of analysis, the BWRO unit is operated continuously for two weeks to evaluate the stability of permeate flow and permeate salinity under single and two-stage modes using a feed TDS of 2000 mg/l. Daily measurements (24 h) were averaged and plotted as daily data. With stable feed salinity and controlled feed water temperature, the average daily of permeate flow and salinity for single stage (1) and two-stage (1–1) are shown in Fig. 11. Throughout two weeks of operation, the RO unit remained stable vis-à-vis its levels of permeate flow and salinity.

Table 5
Statistical test results of agreement between simulated and measured data.

	R^2	EFF
Single-stage (1)		
Permeate flow	0.959	0.946
Permeate salinity	0.951	0.729
Membrane pressure	0.999	0.432
Two-stage (1–1)		
Permeate flow	0.941	0.380
Permeate salinity	0.956	0.676
Membrane pressure	0.999	0.965

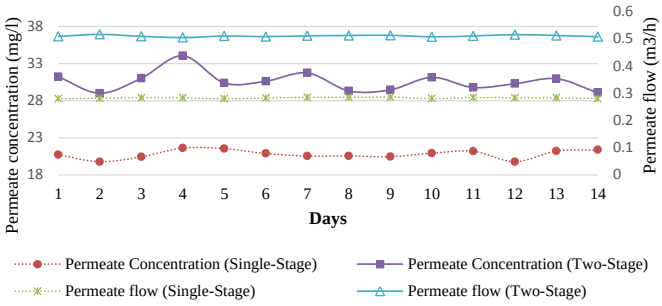

Fig. 11. Measured permeate flow and permeate salinity during 2 weeks of continuous operation under single and two-stage modes.

5.3. Salinity of reject and product water under single & two stage operational modes

Fig. 12 shows the salinity of rejected water and product water at different feed TDS under single and two-stage operation modes. Within the feed TDS range (500–5000 mg/l), the reject TDS range was 851–7384 mg/l and 2065–12,668 mg/l for single stage and two-stage systems, respectively. It can be seen that the product water salinity is always lower than 100 mg/l at single and two-stage modes. This indicates that the membrane type and RO design configuration were fitted to treat the studied range of the feed TDS.

6. Performance of PV power system

Within six months of operation, the net recorded data of solar radiation and subsystem temperatures (ambient, PVtop, PVbottom, battery room and battery body), without any of them missing from 7:30 am to 7:30 pm, was 52 days (624 h). These days were selected as samples to evaluate the status of ambient conditions and their

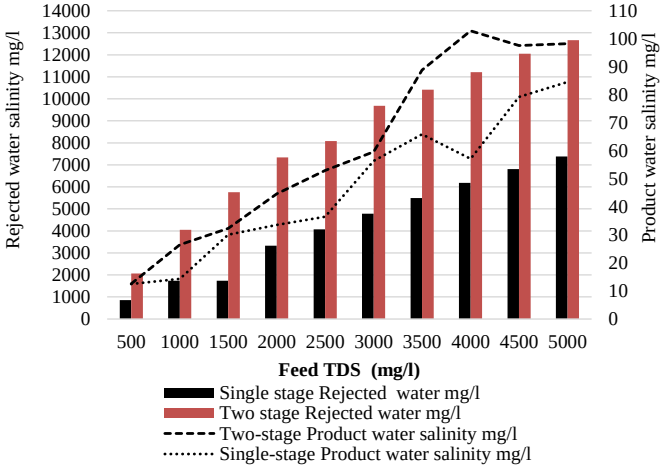

Fig. 12. Reject water and product water salinity versus feed TDS under single and two stage modes.

respective effects on the output of the PV subsystems.

6.1. Status of solar radiation and ambient temperature within the six months of operation

Plotting the time duration (hours or percentage) of solar radiation and temperature would enable us to interpret the output behavior of the PV subsystems at different intervals of solar radiation. It will also help us expect the effect of number of hours at the intervals, which would be of concern to the PV's system performance.

Fig. 13 illustrates the time duration percentage of solar radiation and average ambient temperature at different intervals. The figure is plotted based on 52 days (624 h) of complete recorded data during the daytime.

As shown in the Figure, when solar radiation was in the range of (0–200], (200–400], (400–600], (600–800], (800–1000], and (800–1000] W/m2, the time duration percentage was 33.66%, 19.66%, 14.63%, 13.48%, 14.98%, and 3.58%, respectively. The average ambient temperature was around 32.9 °C when radiation was within (0–200] W/m2, then gradually rising to 42 °C when solar radiations exceeded 800 W/m2. It can be seen that the average ambient temperature was more than or equal 40.7 °C, as the corresponding average solar radiation is exceeding 600 W/m2. The time duration percentage of solar radiation that exceeds 600 W/m2 was about 32% of daytime hours.

In the next round of analysis, the top ten days (120 h) during daytime under clear and overcast sky conditions were assigned. The time duration percentage of solar radiation and average ambient temperature at different solar radiation intervals were plotted and is shown in Fig. 14. The trends of average ambient temperature under both clear and overcast sky conditions are found to be similar. This obtained trend agreed with the temperature trends shown in Fig. 13. Also, it can be seen that the average ambient temperature under an overcast sky is close to the average ambient temperature under a clear sky at the different intervals, with slight differences (less than 1.06 °C).

As shown in Fig. 14, the average ambient temperature was close to or exceeding 40 °C, and the corresponding average solar radiation is more than or equal to 500 W/m2. The time duration percentage of solar radiation that exceeds 500 W/m2 is 48% and 21% of daytime hours under clear and overcast sky conditions, respectively.

Overall, based on Fig. 14; it is confirmed that there are significant number of hours with high average ambient temperature during the daytime under clear sky condition, and a non-neglected number of hours with high average ambient temperature under overcast sky conditions.

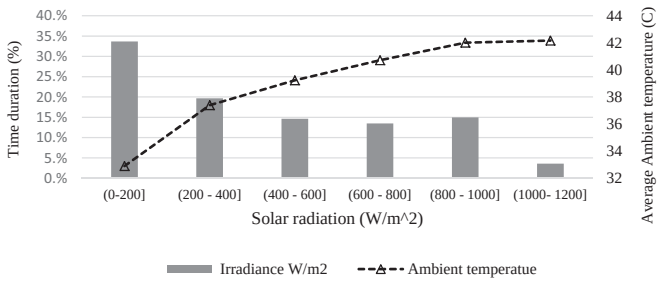

Fig. 13. Time duration percentage and average ambient temperature versus different intervals of solar radiation during day time of 52 days.

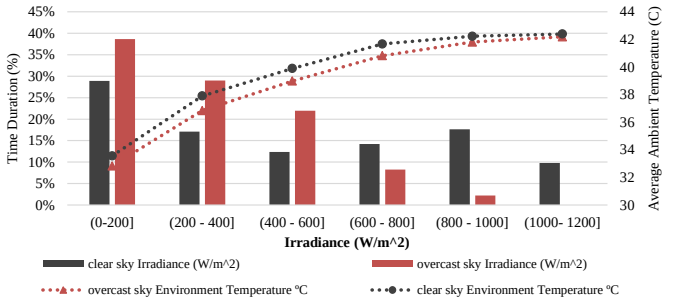

Fig. 14. Time duration (%) and average ambient temperature versus solar radiation intervals using top 10 days of clear and overcast sky conditions.

6.2. Status of temperature at different components of PV system

Higher solar radiation is preferred as it increases the power output of the PV system. However, under higher levels of solar radiation, the temperature of PV modules and batteries will increase and causes deficiency on the PVoutput power, battery autonomy, and the life span of the battery. So, plotting the time duration percentage at different intervals of the temperature would enable us to interpret the output behavior of the subsystems.

Fig. 15 (A–B) shows the hours and percentage of time duration, respectively, at different temperature intervals for ambient, battery room, battery body, and PVtop and PVbottom panels using 52 days of complete records during daytime (total of 624 h).

During the day, the time duration percentages of ambient temperature at [26–35 °C] and [36–45 °C] temperature intervals were 27.83% and 71.43%, respectively, and it rarely exceeded 45 °C (0.75%). It is clearly seen that the dominant ambient temperature interval during daytime was [36–45 °C].

The temperature of PVtop module was relatively higher compared to PVbottom, but both were comparatively similar at noon. PVtop and PVbottom temperatures exceeding 45 °C were recorded at 245.59 h (39.4%) and 203.43 h (32.5%), respectively. Therefore, it can be concluded that there is a significant number of hours of high PV module temperature that can affect the PVoutput

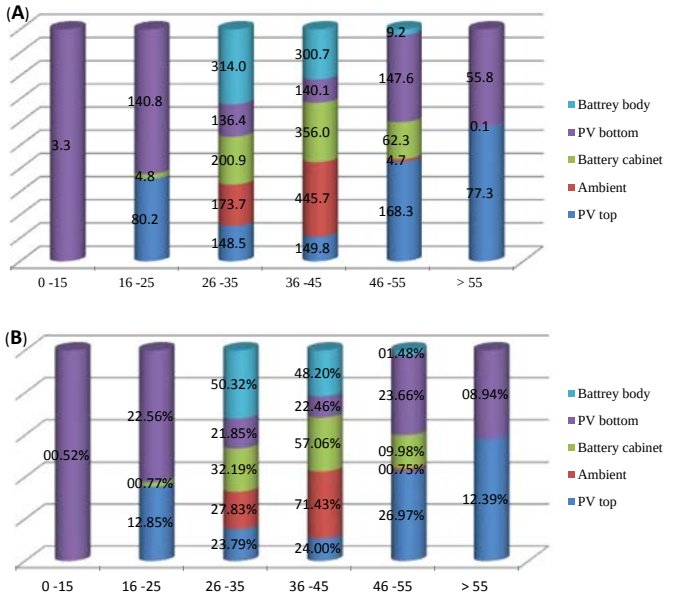

Fig. 15. (A–B): Time duration versus different temperature intervals for ambient, battery body and room, PV_{top} and PV_{bottom} in hours and percentage respectively.

power. During sunset, the PVtop temperature continues to drop to its lowest point within (16–25)°C. During early mornings, although the ambient temperature was at least 26 °C, the lowest recorded PVbottom temperature was 14 °C, at a time duration of 3.3 h (0.52%) and interval (0–15). Then, the temperature rises rapidly to beyond 60 °C after sunrise.

A battery room temperature that is less than 25 °C is quite rare, where the recorded total time is 4.8 h (0.77%). Battery room temperature that exceeds 45 °C sometimes occurred, where the total recorded time was 62 h (10%). Battery room temperatures in the range of 26–35 °C were recorded at 201 h (32.19%), and mostly within the range of 36–45 °C, at 356 h (57.06%). The battery body temperature during daytime is always more than 25 °C, and rarely exceeds 45 °C, with total recorded time of 9.2 h (1.48%). The battery body temperatures in the range of 26–35 °C and 36–45 °C were recorded at 314 h (50.32%) and 300.7 h (48.2%), respectively. Therefore, it can be concluded that there is a significant number of hours of high battery body/battery room temperatures that could affect the performance of the batteries.

For a more in depth analysis, the top ten days (120 h) under clear and overcast sky conditions during daytimes were assigned. The time duration percentage of ambient, battery room, battery body, PVtop and PVbottom module at different temperature intervals are shown in Fig. 16.

Under clear sky condition during the day, time duration percentages of ambient temperature at [26–35 °C] and [36–45 °C] temperature intervals are 20.30% and 77.26%, respectively, and it rarely exceeded 45 °C (2.44%), while during daytimes under overcast sky conditions, the time duration percentages of ambient temperature at [26–35 °C] and [36–45 °C] temperature intervals are 44.41%, 55.59% respectively. Therefore, it can be concluded that the dominant ambient temperature interval during the day was [36–45 °C] under clear and overcast sky conditions.

As shown in Fig. 16, time duration percentage of (PVtop, PVbottom) module temperatures exceeding 45 °C under clear and overcast sky conditions were (52.22%, 36.46%) and (20.30%, 6.66%), respectively. It can also be seen that the time duration percentage of (battery room, battery body) temperatures exceeding 35 °C under clear and overcast sky conditions are (79.56%, 72.12%) and (47.93%, 9.88%), respectively.

Based on the facts learned from Figs. 15 and 16, it is confirmed that there is a significant number of hours of high PV module temperature (exceeding 45 °C) and high battery room and body temperatures (exceeding 35 °C) that influences the PVoutput power and battery performance.

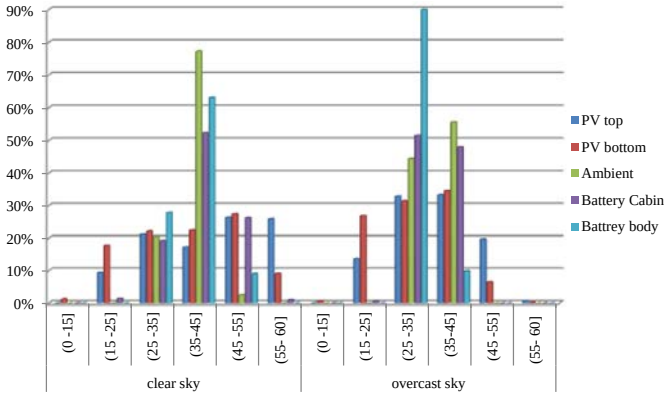

Fig. 16. Time duration percentage versus different temperature intervals for top 10 days under clear and overcast sky conditions.

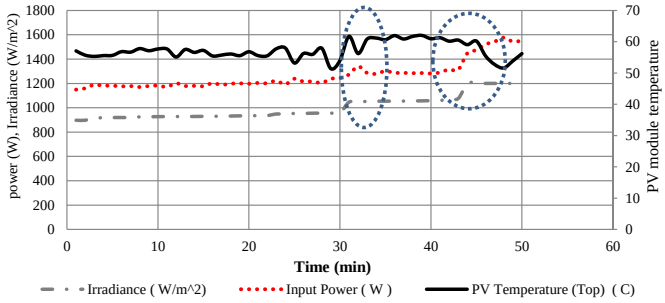

Fig. 17. Effect of solar radiation and PV module temperature on PV_{output} power.

6.3. Factors affecting optimal PVoutput power

Solar radiation and temperature are crucial towards PVoutput power. For this purpose, one hour (60 min) of measured data for these parameters was chosen as a sample. Fig. 17 illustrates the effect of solar radiation and PVtop module temperature on the PVoutput power at noon during a clear day.

As shown in the figure, when solar radiation increased from 912 W/m2 to 1200 W/m2, the PVoutput power increased from 1181 W to 1520 W. This means higher solar radiation is preferred for the increase of PVoutput power. At constant solar radiation of 1200 W/m2, it is shown that the PVoutput power could increase from 1520 W to 1576 W, due to the decrease in the PVtop module temperature from 60 to 51 °C. This means that the optimal PVoutput power could be achieved at higher solar radiation and lower PV module temperatures concurrently.

6.4. Performance ratio of PV power system

The performance ratio (PR) is one of the most important parameters for evaluating the efficiency of a PV power system. It is the ratio between the actual and theoretical electrical energy production. The monthly performance ratio (PR) is shown in Fig. 18. Records from November and December showed lower PR due to losses in cabling malfunction (faulty in the cable size). It results in the system regularly ceasing operations, especially during afternoons when the ambient temperature is high. Switching the cable subsequently increased the PR of the system.

6.5. Results of two weeks of continuous operation of the PV-BWRO desalination system

In this round of analysis, the PV-BWRO test unit is operated by the PV power system continuously for two weeks during daytime

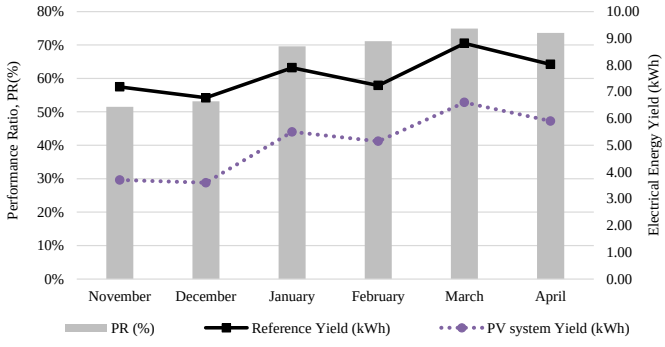

Fig. 18. Monthly performance ratio, reference and actual monthly average electrical energy yield of 2 kW_p PV system.

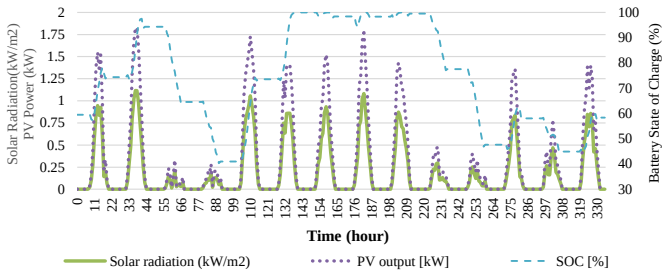

Fig. 19. Characteristics of solar radiation, PV output and battery state of charge during two weeks of daytime operation.

(10 h). The RO unit was operated at feed TDS of 2000 mg/l under a single-stage mode.

Fig. 19 illustrates the characteristics of hourly solar radiation, PVoutput power, and the battery's state of charge. It can be seen that there is a clear harmony between PVoutput power and solar radiation during both clear sky and overcast days observed in the figure. During high solar radiation days, the battery is charged, keeping the battery state of charge (SOC) ~100%. During low solar radiation days, the SOC could be reduced to 40%. This happened after two consecutive cloudy days, where the SOC decreased from 97.5% to 40%.

Fig. 20 illustrates the characteristics of hourly solar radiation, RO load, and water production. On the whole, the RO load and water production remained stable under different sky conditions, where the permeate flow was around 4.5 l/min and the RO load was around 0.6 kW. The RO load remains constant during operating hours, because it was consuming energy from the battery bank, which was charged by solar radiation and PV panels. This confirms that the PV system is able to supply the load without any disturbance during two weeks of operation.

7. Effect of battery room temperature conditions on battery bank autonomy

In this section, a test will shed light on the influence of battery room temperature conditions on the battery bank's autonomous performance. The batteries were purchased in March 2012. Since then, the battery bank was placed in the same room, without any modification to the room's conditions. A photo of battery bank room is shown in Fig. 21. It was made from stainless steel sheet to withstand the weight of the batteries, due to the fact that each of them weighs over 60 kg.

It should be pointed out that the battery's autonomy hours, as obtained from the HOMER simulation tool, was 46.5 h. Unfortunately, the battery's autonomy performance was not tested in

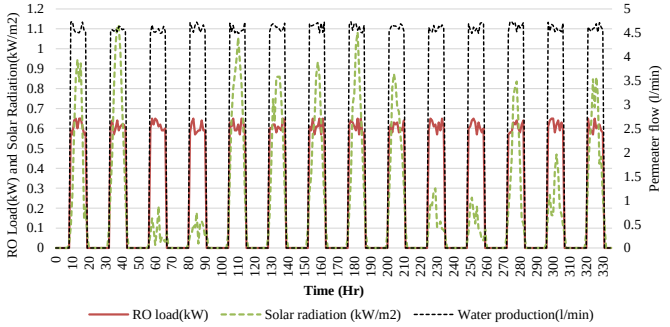

Fig. 20. Characteristics of hourly RO load, water production and solar radiation during two weeks of daytime operation.

Fig. 21. Photo of battery bank room.

March 2012 when the batteries were still new for comparison with the simulated autonomy hours. This was because the delivery of the RO unit was delayed for about a year, and was finally delivered in April 2013. However, battery autonomy performance was tested only in March 2014 and March 2015. The test was performed under daytime and nighttime modes. To start the test, the battery bank was fully charged (100%), first by the PV system, followed by the RO load being allowed to rely on battery power alone.

7.1. Comparison of autonomy performance between daytime and nighttime in March 2014

At this stage, we need to evaluate the status of battery autonomy performance in March 2014 after two years of battery room temperature conditions (March 2012–March 2014).

7.1.1. Daytime operation mode

The battery autonomy test began in 13/3/2014, and was completed in 14/3/2014. As shown in Fig. 22, the battery bank managed to power the load from 7:30 am to 7:30 pm in the first day, and again during the next day, from 7:30 am, until the RO system ceased operations at 5:30 pm. The total autonomy hours were 22 h. During the daytime duration of the autonomy test, the maximum and minimum recorded temperature of the battery room were 54 °C and 27 °C, respectively, while the average battery room temperatures for the 1st and 2nd day were found to be 46 °C and 47 °C, respectively.

7.1.2. Night time operation mode

The battery discharge test began on 8th March 2014, and was completed the next day. During the test days, the battery bank powered the load from 7:30 pm to 7:30 am in the first day, and started again the next day from 7:30 pm until the RO system was shutdown at 7:24 am. The total autonomy hours were 23 h and

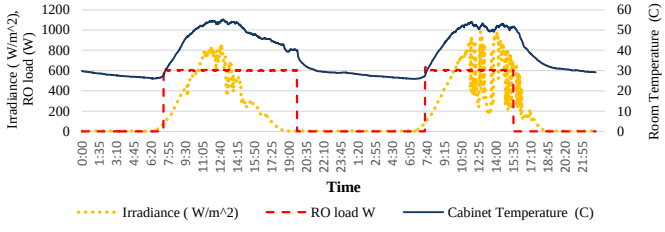

Fig. 22. Battery autonomy performance during daytime tested in 13-14-Mar-2014.

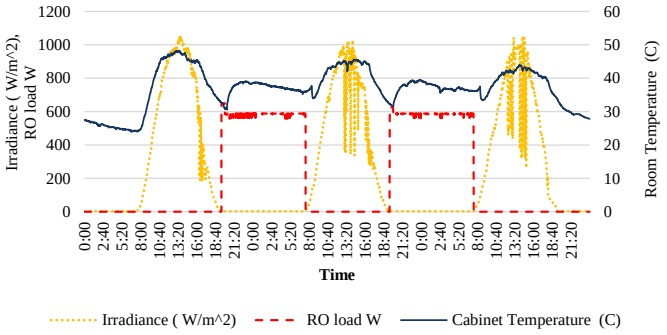

Fig. 23. Battery autonomy performance during nighttime tested in 08/09-Mar-2014.

54 min, as shown in Fig. 23. During the nighttime duration of the autonomy test, the maximum and minimum recorded temperatures of the battery room were 39 °C and 31 °C, respectively, while the average battery room temperatures for the 1st and the 2nd day were found to be 37.05 °C and 37.12 °C, respectively.

Based on Figures 22 and 23, the battery bank autonomy hours during daytime and nighttime modes were ~22 h and ~24 h, respectively. This reveals that the effect of battery room temperature conditions during the day resulted in a 2-h reduction in battery autonomy compared to the nighttime test results.

7.2. Comparison of autonomy performance between daytime and nighttime in March 2015

At this stage, we need to evaluate the status of battery autonomy performance in March 2015 after three years of battery room temperature conditions (March 2012 to March 2015).

7.2.1. Daytime operation mode

The test was performed in (25/3/2015). The autonomy test results showed that the battery bank was able to power the load for only 10 h and 55 min, as shown in Fig. 24. During the autonomy test hours, the maximum, minimum, and average recorded temperature of the battery room were 55.3 °C, 28.4 °C, and 48.77 °C respectively.

To confirm the accuracy of the autonomy results, the test was repeated in (31/3/2015). Again, the total autonomy hours were found to be 11 h and 33 min, as shown in Fig. 25, which is close to the results shown in Fig. 24. During the autonomy test hours, the maximum, minimum, and average recorded temperature of the battery room were 55.6 °C, 27 °C, and 46.81 °C, respectively.

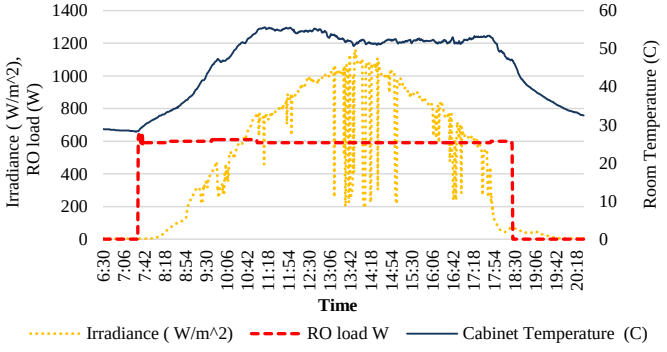

Fig. 24. Battery autonomy performance during daytime tested in 25/3/2015.

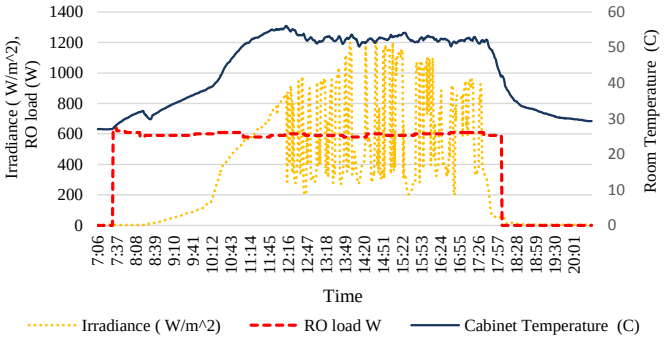

Fig. 25. Battery autonomy performance during daytime tested in 31/3/2015.

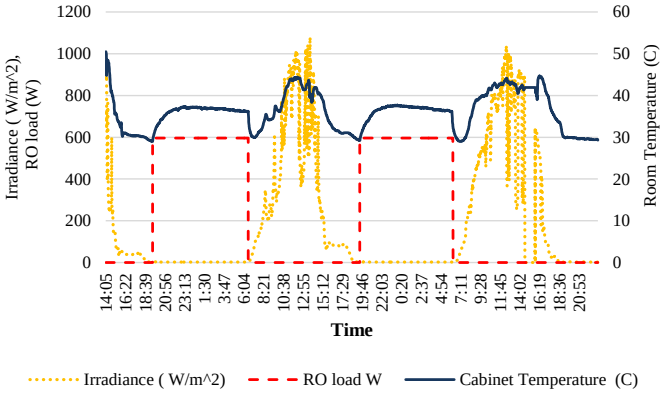

Fig. 26. Battery autonomy performance during nighttime tested in 23/24-Mar-2015.

7.2.2. Night time operation mode

The autonomy test began in (23rd March 2015), and was completed the next day. The total running time of the RO load was 22 h and 43 min, as shown in Fig. 26. During the nighttime duration of the test days, the maximum and minimum recorded temperatures of the battery room were 37.5 °C and 29 °C, respectively.

Based on Figures 24–26, the battery bank autonomy hours were ~11 h and ~23 h under daytime and nighttime operation modes, respectively. Therefore, it can be concluded that the autonomy hours showed a significant deficiency during daytime compared to nighttime, due to the high battery room's temperature.

7.3. Comparison of autonomy performance between March 2014 and March 2015

In this round of analysis, the comparison of autonomy performance between March 2014 and March 2015 during daytime and nighttime will be verified.

7.3.1. Daytime room temperature

Under the daytime operation mode, and based on figures (22), (24) and (25), the battery bank autonomy hours were ~22 h and ~11 h in March 2014 and March 2015, respectively. Therefore, it can be concluded that a 50% reduction in autonomy hours is obtained within one year of battery room temperature conditions. This means that the battery room temperature conditions are significantly inappropriate. Shading the room and applying a ventilation option inside the room could solve this problem.

7.3.2. Nighttime room temperature

Under nighttime operation mode and based on Figures (23 and

26), the battery bank autonomy hours were (23 h and 54 min) and (22 h and 43 min) in March 2014 and March 2015, respectively, resulting in a 1-h reduction. This marginal autonomy reduction could be attributed to the ambient temperature during nighttime, which is not far from the standard temperature (25–30 °C) for optimal battery performance.

It could also be concluded that even though the battery bank showed a significant reduction of autonomy hours during the day due to high room temperature, it still performed well under nighttime temperature conditions.

Overall, a significant number of hours with high temperatures during daytimes affected the battery autonomy performance negatively, and this effect will be compounded annually. Therefore, the thermal conditions of the battery room must be managed to maintain the batteries' temperature as close as possible to the standard battery temperature for increased and reliable performance.

8. Cost details of PV-BWRO test unit for research purpose

Table 6 summarizes the prices of the system's components, the total cost of the PV system & the RO unit, on top of the cost of the data acquisition system. The PV system shows the highest cost (62,320RM), followed by the data acquisition system (45,000RM), and finally, the RO unit (20,300RM). As shown in Table 6, the total initial cost of the BWRO desalination unit powered by a 2 kWp PV power system for research purposes is (127,620RM), which is equivalent to 30,000$ [1$ = 4.26 MYR].

9. Conclusion

In this study, the design and construction of a small scale PV-BWRO desalination test unit was performed. Six months of desalination test unit operation under different modes were carried out. The outcomes from this study are:

- A 2 kWp PV system was purchased based on the allocated fund. The design results showed that a 2 kWp PV system could only power a 600 W RO load under Malaysia climate. Then, the BWRO desalination unit is designed based on a 600 W load, feed TDS of 2000 mg/l, and permeate TDS of less than 50 mg/l. The design results showed that (4″x40″ TW30-4040) membrane type and two-stage (with one membrane element at each stage) are the optimum BWRO design choices.
- During the experimental test, the RO unit is pushed to operate under a feed salinity of up to 5000 mg/l under single and two-stage configurations. The experimental results showed that even though the BWRO unit is designed under a feed TDS of 2000 mg/l, it is still able to produce permeate flow with acceptable permeate salinity (less than 50 mg/l) when the feed TDS is under 5000 mg/l. During two weeks of continuous run, the stable levels of permeate flow and permeate salinity were observed. The PV system was able to supply the load without any significant disturbance. Operating the PV-BWRO system for 10 h during the day produced 5.1 m3 of fresh water at a specific energy of 1.1 (kWh/m3).
- Under experimental validation, the measured and simulated values showed a satisfactory to excellent agreement under different feed salinity tests for permeate flow, permeate salinity, and RO unit pressure. So, the validation results ensured the appropriateness of assumptions and procedures adopted in the design and sizing of a PV-BWRO system.
- Comparing the autonomy performance between daytime and nighttime in March 2014, the battery bank autonomy hours during daytime and nighttime modes were 22 h and ~24 h, respectively. This reveals that the effect of battery room temperature conditions during daytime resulted in a 2-h reduction in the battery autonomy compared to the nighttime test results.
- Comparing the autonomy performance between daytime and nighttime in March 2015, the battery bank autonomy hours were about 11 h and ~23 h under daytime and nighttime operation modes, respectively. So, it can be concluded that the autonomy hours showed a significant deficiency during daytime compared to nighttime, due to the high temperature of the battery room.
- Comparing the autonomy performance between March 2014 and March 2015, it can be concluded that even though the battery bank showed a significant reduction of autonomy hours during daytime due to high room temperature; it is still able to perform well when the room is under nighttime temperature conditions.

Overall, it is found that during daytimes, there are significant number of hours of high PV module temperature (exceeding 45 °C)

Table 6
Detailed components prices and the initial cost of PV-BWRO system for research purpose.

Component	Unit price (RM)	Unit	Total (RM)
PV modules	910	16	14,560
Mounting structure	–	–	2500
Charge controller	2500	1	2500
Inverter	11,200	1	11,200
Battery	1445	8	11,560
Wiring and other accessories	–	–	10,000
Transportation	–	–	10,000
Total PV system cost			62,320
Pressure vessel	2400	2	4800
Membrane element	700	2	1400
Feed pump	2000	1	2000
Multimedia Filter	1500	1	1500
Sediment Filter	500	1	500
Feed pump	2000	1	2000
Water tank	1100	1	1100
Structure	–	–	2000
Piping and other accessories	–	–	5000
Total BWRO system cost			20,300
Measurement and data acquisitions (PV system and BWRO unit)		–	45,000
Total PV-BWRO system cost			127,620

and high battery temperature conditions (exceeding 35 °C) that could negatively affect the output power and battery autonomy, respectively. This negative effect is compounded annually; therefore, high attention to the thermal regulation of PV modules and battery bank conditions is essential.

Acknowledgments

The work is financially supported by the research grant (UKM-GUP-BTT-07-29-185). We hereby wish to acknowledge the financial assistance of the National University of Malaysia, Malaysia.

References

[1] UNICEF & WHO, Progress on Drinking-water and Sanitation–2012 Update, launched on, 6 March 2012, http://www.unicef.org/media/files/JMPreport2012.pdf.
[2] A.M. Abdulsalam, I. Ithoi, H.M. Al-Mekhlafi, A. Ahmed, J. Surin, J.-W. Mak, Drinking water is a significant predictor of Blastocystis infection among rural Malaysian primary schoolchildren, Parasitology 139 (2012) 1014–1020.
[3] C. Fritzmann, J. Löwenberg, T. Wintgens, T. Melin, State-of-the-art of reverse osmosis desalination, Desalination 216 (2007) 1–76.
[4] M. Li, Reducing specific energy consumption in Reverse Osmosis (RO) water desalination: An analysis from first principles, Desalination 276 (2011) 128–135.
[5] N. Voros, C. Kiranoudis, Z. Maroulis, Solar energy exploitation for reverse osmosis desalination plants, Desalination 115 (1998) 83–101.
[6] A. Zhu, P.D. Christofides, Y. Cohen, Effect of thermodynamic restriction on energy cost optimization of RO membrane water desalination, Ind. Eng. Chem. Res. 48 (2009) 6010–6021.
[7] T. Espino, B. Penate, G. Piernavieja, D. Herold, A. Neskakis, Optimised desalination of seawater by a PV powered reverse osmosis plant for a decentralised coastal water supply, Desalination 156 (2003) 349–350.
[8] M. Alghoul, P. Poovanaesvaran, K. Sopian, M. Sulaiman, Review of brackish water reverse osmosis (BWRO) system designs, Renew. Sustain. Energy Rev. 13 (2009) 2661–2667.
[9] S. Abdallah, M. Abu-Hilal, M. Mohsen, Performance of a photovoltaic powered reverse osmosis system under local climatic conditions, Desalination 183 (2005) 95–104.
[10] J.H. Lindemann, Wind and solar powered seawater desalination applied solutions for the Mediterranean, the middle east and the Gulf countries, Desalination 168 (2004) 73–80.
[11] D. Herold, A. Neskakis, A small PV-driven reverse osmosis desalination plant on the island of Gran Canaria, Desalination 137 (2001) 285–292.
[12] E. Tzen, K. Perrakis, P. Baltas, Design of a stand alone PV-desalination system for rural areas, Desalination 119 (1998) 327–333.
[13] P. Sarkar, D. Goswami, S. Prabhakar, P. Tewari, Optimized design of a reverse osmosis system with a recycle, Desalination 230 (2008) 128–139.
[14] J. Ayoub, R. Alward, Water requirements and remote arid areas: the need for small-scale desalination, Desalination 107 (1996) 131–147.
[15] A. Joyce, D. Loureiro, C. Rodrigues, S. Castro, Small reverse osmosis units using PV systems for water purification in rural places, Desalination 137 (2001) 39–44.
[16] M. Thomson, D. Infield, Laboratory demonstration of a photovoltaic-powered seawater reverse-osmosis system without batteries, Desalination 183 (2005) 105–111.
[17] P. Poovanaesvaran, M. Alghoul, K. Sopian, N. Amin, M. Fadhel, M. Yahya, Design aspects of small-scale photovoltaic brackish water reverse osmosis (PV-BWRO) system, Desalination Water Treat. 27 (2011) 210–223.
[18] A. Maurel, Desalination by reverse osmosis using renewable energies (solar-wind) Cadarche centre experiment, in: Seminar on New Technologies for the Use of Renewable Energies in Water Desalination, Athens, 1991, pp. 26–28.
[19] J. Andújar Peral, A. Contreras Gómez, J. Trujillo, IDM-Project: results of one year of operation, in: Seminar on New Technologies for the Use of Renewable Energies in Water Desalination, Athens, 1991, pp. 26–28.
[20] S. Kehal, Reverse osmosis unit of 0.85 m3/h capacity driven by photovoltaic generator in South Algeria, in: Proceedings of the New Technologies for the Use of Renewable Energy Sources in Water Desalination Conference, Session II, 1991, pp. 8–16.
[21] P.C.M. de Carvalho, D.B. Riffel, C. Freire, F.F.D. Montenegro, The Brazilian experience with a photovoltaic powered reverse osmosis plant, Prog. Photovolt. Res. Appl. 12 (2004) 373–385.
[22] Z. Al Suleimani, V.R. Nair, Desalination by solar-powered reverse osmosis in a remote area of the Sultanate of Oman, Appl. Energy 65 (2000) 367–380.
[23] A. Al-Karaghouli, L.L. Kazmerski, Economic Analysis of a Brackish Water Photovoltaic-operated (BWRO-pv) Desalination System, 2010.
[24] L. Garcı, Renewable energy applications in desalination: state of the art, Sol. energy 75 (2003) 381–393.
[25] D. Herold, V. Horstmann, A. Neskakis, J. Plettner-Marliani, G. Piernavieja, R. Calero, Small scale photovoltaic desalination for rural water supply-demonstration plant in Gran Canaria, Renew. Energy 14 (1998) 293–298.
[26] W. Gocht, A. Sommerfeld, R. Rautenbach, T. Melin, L. Eilers, A. Neskakis, et al., Decentralized desalination of brackish water by a directly coupled reverse-osmosis-photovoltaic-system-a pilot plant study in Jordan, Renew. Energy 14 (1998) 287–292.
[27] S. Alajlan, M. Smiai, Performance and development of PV-plant for water pumping and desalination for remote area in Saudi Arabia, Renew. energy 8 (1996) 441–446.
[28] W. Qi, J. Liu, P.D. Christofides, A distributed control framework for smart grid development: energy/water system optimal operation and electric grid integration, J. Process Control 21 (2011) 1504–1516.
[29] W. Qi, J. Liu, P.D. Christofides, Supervisory predictive control for long-term scheduling of an integrated wind/solar energy generation and water desalination system, Control Syst. Technol. IEEE Trans. on 20 (2012) 504–512.
[30] H. Mahmoudi, S. Abdul-Wahab, M. Goosen, S. Sablani, J. Perret, A. Ouagued, et al., Weather data and analysis of hybrid photovoltaic–wind power generation systems adapted to a seawater greenhouse desalination unit designed for arid coastal countries, Desalination 222 (2008) 119–127.
[31] M. Hussin, A. Yaacob, R. Rahman, Z. Zain, S. Shaari, A. Omar, Monitoring results of Malaysian building integrated PV Project in Grid-connected photovoltaic system in Malaysia, Energy Power 2 (2012) 39–45.
[32] T. Lambert, P. Gilman, P. Lilienthal, Micropower system modeling with HOMER, Book: integration of alternative sources of energy, in: F.A. Farret, M.G. Simões (Eds.), John Wiley & Sons, Inc., 2006, pp. 379–417, http://dx.doi.org/10.1002/0471755621 ch.15.
[33] Reverse Osmosis System Analysis (ROSA) @ http://www.dowwaterandprocess.com.
[34] Stanton A. Glantz, Bryan K. Slinker, Primer of Applied Regression and Analysis of Variance, second ed., McGraw-Hill, 2001.
[35] D. Mayer, D. Butler, Statistical validation, Ecol. Model. 68 (1993) 21–32.
[36] A.K. Yadav, S. Chandel, Tilt angle optimization to maximize incident solar radiation: a review, Renew. Sustain. Energy Rev. 23 (2013) 503–513.